ELSEVIER

Contents lists available at ScienceDirect

## Earth and Planetary Science Letters

www.elsevier.com/locate/epsl



# Earth's inner core rotation, 1971 to 1974, illuminated by inner-core scattered waves



Wei Wang\*, John E. Vidale

Department of Earth Sciences, University of Southern California, United States of America

#### ARTICLE INFO

Article history:
Received 12 June 2021
Received in revised form 13 September 2021
Accepted 16 September 2021
Available online 22 October 2021
Editor: H. Thybo

Dataset link: https://github.com/JohnVidale/LASA\_data

Keywords:
Earth's inner core
Inner-core scattered waves
Inner-core differential rotation
Inner core wobble

#### ABSTRACT

The solid inner core is at the center of the Earth, gravitationally held within the liquid outer core. It is one of the most dynamic parts of Earth's interior. Since the initial claim of inner core differential rotation relative to the mantle, its existence and rate have been challenged for over two decades. Here, we re-examine the seismic records of two megaton nuclear tests in Novaya Zemlya, Russia, three years apart, from the Large Aperture Seismic Array in Montana, USA. Using an improved static time correction from an antipodal earthquake, we refine the resolution of the beamforming of PKiKP and its inner-core scattered coda. Then, we measure the slight time shifts (tenths of seconds) between the inner-core-scattered waves from the two events with moving-time-window cross-correlation. Applying a novel back-projection method, we locate the inner-core regions that scatter the energy within the PKiKP coda based on its slowness and the lapse time. We then measure the inner core rotation, first assuming alignment with Earth's rotation axis, then finding the best-fitting differential rotation axis with a grid search. The rotation rates here are robust and consistent across the many scattered arrivals throughout the inner core scattering wavetrain. Our results indicate 0.10°/year inner core super-rotation rate from 1971 to 1974 aligned with Earth's rotation axis, or 0.125°/year with the rotation axis tilting about 8° from the Earth's rotation axis, which yields a marginally better fit to the observed time shifts.

© 2021 Elsevier B.V. All rights reserved.

## 1. Introduction

Earth's solid inner core (IC), which grows from the slow solidification of the liquid outer core (OC), is a central but poorly understood frontier of Earth sciences. The latent heat and light elements released during the solidification drive the convection in the OC, which powers the geodynamo for the Earth's geomagnetic field [Gubbins, 1981; McFadden and Merrill, 1984; Glatzmaier and Roberts, 1995]. The IC is gravitationally held under the liquid OC, and differential rotation of the IC from the electromagnetic torque produced by the OC convection is possible [Glatzmaier and Roberts, 1995]. Investigation of the motion of the IC may improve the knowledge of the formation and evolution of the IC and OC and enhance the understanding of Earth's geomagnetic field.

Differential rotation of the IC was first apparent in the three-dimensional numerical simulations of the geodynamo [Glatzmaier and Roberts, 1996], and then corroborated by the seismological observations of the systematic increase of the PKPbc (a compressional wave bottoming in the lower outer core) – PKIKP (a com-

\* Corresponding author.

E-mail address: weiwang053@gmail.com (W. Wang).

pressional wave refracted in the IC) differential travel times from 1967 to 1995 [Song and Richards, 1996]. Since then, many ensuing studies of the IC differential rotation have inferred similar superrotation, using various seismological data, i.e., transmitted body waves [Creager, 1997; Zhang et al., 2005; Yang and Song, 2020a], back-scattered body waves [Vidale et al., 2000; Vidale, 2019], and normal modes [Laske and Masters, 2003]. More recent works have advanced models that are quite diverse, including super-rotation rates varying from about 1° per million years to 3° per year [Song and Richards, 1996; Su et al., 1996; Creager, 1997; Laske and Masters, 2003; Zhang et al., 2005; Cao et al., 2007; Waszek et al., 2011; Yang and Song, 2020a], accelerating rotation [Lindner et al., 2010], and strongly fluctuating or oscillating rotation rates [Ding and Chao, 2018; Tkalčić et al., 2013]. At the same time, the very existence of the IC differential rotation has been in debate. Some studies argued the measured PKPbc-PKIKP differential travel times may represent mislocations of the earthquakes [Souriau, 1998a, 1998b; Poupinet et al., 2000] or heterogenous structure along the raypaths [Souriau and Poupinet, 2000]. The time-varying PKiKP arrivals (a compressional wave reflected at the IC boundary) might indicate localized changes at the inner core boundary (ICB) [Wen, 2006; Xin et al., 2015; Yao et al., 2015, 2019]. Consequently, some

studies [Yao et al., 2019; Mäkinen and Deuss, 2011; Deuss, 2014] claim that some of the best resolved datasets cannot be interpreted as the pure super-rotation.

Vidale et al. [2000] first used inner-core scattered waves (ICS) to estimate a rotation rate of  $\sim\!0.15^\circ/\text{year}$ . In his recent study [Vidale, 2019], using correlation-based static corrections for the Large Aperture Seismic Array (LASA) stations, the resolution of the beamforming is improved. The time shifts between the hand-selected coherent blips from the two nuclear tests are used to estimate a rotation rate that is about half of the previous study,  $\sim\!0.07^\circ/\text{year}$ . As controversy about the reality of IC rotation persists, in this study, we take into account the depths of scatterers and objectively threshold the significant signals and time shifts. We also consider the case that the pole of differential rotation may differ from Earth's pole of rotation.

#### 2. Data and method

The IC scattered waves, compared to the transmitted (PKIKP) or reflected compressional (PKiKP) waves, are more precise and sensitive to a small IC rotation [Vidale, 2019]. Also, the systematic changes of time shifts from the numerous IC scatterers provide a wide spatial coverage and many measurements of the IC interior compared to the limited measurements from transmitted waves. The disadvantage of the IC scattered waves is that the observation of the short-period ICS relies on the geometry and aperture of the network, and sufficiently favorable data are rarely recorded. Also, large events and precise repeatability are required to measure the time shifts.

In this study, we use the seismic records of a pair of megaton nuclear tests in northern Novaya Zemlya, Russia in September 1971 and August 1974, recorded at  $\sim\!60^\circ$  distance on LASA in Montana, USA. LASA comprised up to 525 vertical-component stations across a 200-km aperture, emplaced in 60-m boreholes in firm ground (see Fig. 1, Frosch and Green, 1966). 311 stations recorded the first event and 205 the second one, with 199 in common. We will use in this study the common 199 stations to analyze the IC motion. The unsurpassed resolution of about 0.01 s/km slowness for LASA provides this fortunate chance to locate the scatterers within the IC, which refine estimation of the IC rotation.

We bandpass filter the seismograms to retain only 1 to 3 Hz energy; most is 1 to 2 Hz, centered at about 1.5 Hz. A beamforming approach including static shift corrections is applied to all the available LASA stations, then envelopes are formed for each incident wave slowness vector [Vidale, 2019]. The static shifts, on the order of tenths of seconds, correct the wavefront distortion due to crust and mantle structures under LASA. The statics, refined for this paper, were estimated by cross-correlation alignment with iasp91 predictions [Kennett and Engdahl, 1991] of the PKIKP phases for an earthquake near the antipode [Vidale, 2019].

## 3. Time shift measurement by cross-correlation

In Vidale [2019], the time shifts between the two explosions are computed from the instantaneous phase difference of stacks at common slownesses and back-azimuths. In this study, we apply a moving-time-window cross-correlation (CC) approach to better measure the time shifts between the two beamformed stacks. To robustly measure the time shifts, we select a 4-second time window with up to a 0.4-second shift to search for the maximum CC. Compared with the method in Vidale [2019], the CC measurements are more consistent in the large-amplitude, high-similarity regime, and smoother and more robust in the small-amplitude, low-similarity regime (see Fig. 2A & 2B and Figure S1).

In our moving-time-window CC approach, we again interpret only the data that surpasses the quality thresholding criteria from

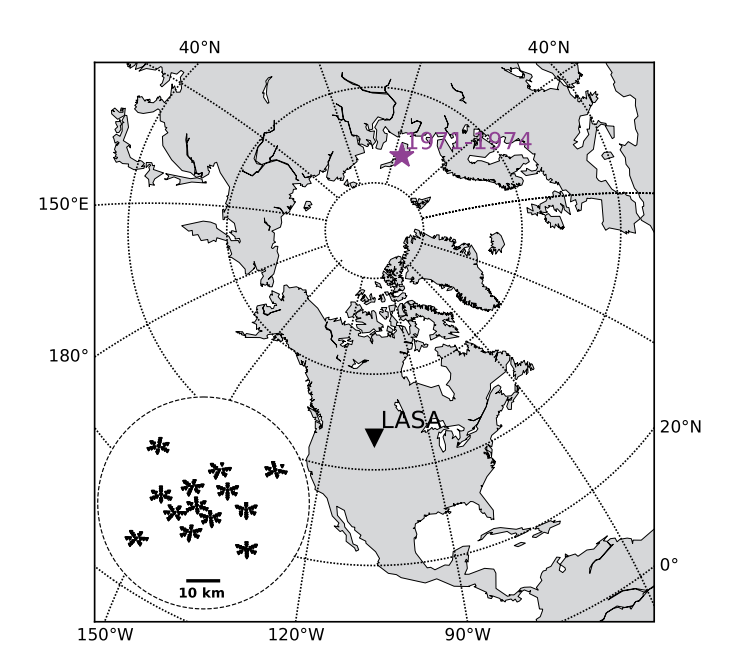


**Fig. 1.** The locations of the twin nuclear tests and LASA. The black triangle marks the location of LASA and the dashed circle highlights the geometry of the common 199 inner-ring LASA stations used in this study. The magenta star shows the location of the twin nuclear tests used in this study. (For interpretation of the colors in the figure(s), the reader is referred to the web version of this article.)

Vidale [2019]. We compute the average of the envelope amplitudes of the stacks and the envelope amplitude ratios between the traces for the two events at the same slownesses and backazimuths. In this study, we use two alternate approaches to search for the blips that are high-energy and highly coherent (HEHC). First, we select the numerous HEHC points using a generous criterion; CC coefficients larger than 0.8, average amplitudes larger than 40% of the peak values of global beams, and amplitude ratios between the stack windows for the two explosions between 0.2 and 1.8. Fig. 2 shows the results from imposing these criteria for the East-West (E-W) slowness slice with North-South (N-S) slowness of 0.01 s/km. Second, we search for the more limited number of most robust HEHC points using the more stringent criterion of CC coefficients larger than 0.9, average amplitudes larger than 0.5, and amplitude ratios within 0.5 and 1.5 to find fewer but more robust time-shift estimates.

## 4. Array processing approach

The HEHC points each have a characteristic arrival time, back-azimuth, and slowness. Based on these measurements, we back-project the raypaths of the HEHC points to their corresponding scattering locations (see Fig. 3) [Frost et al., 2013; Vidale and Wang, 2020]. The basic idea is developed and improved from the techniques of Wen [2000] and Cao and Romanowicz [2007], which use beams of PKP precursors to determine the locations of scatterers in the lower mantle based on a single scattering assumption. Energy at a specific time prior to the PKP arrival might arise from scattering anywhere on "isotime" surfaces on both source- and receiver-sides of the lower mantle. Adding the slowness vector of the precursor energy, in addition to its relative time prior to PKP arrival, constrains the scatterer location to a point rather than just somewhere on a surface. This approach has also been used to estimate isolated scatterer locations in the mantle [Frost et al., 2013].

In the case that the IC moves relative to the mantle, the scatterers within the IC move with the IC. Consequently, the energy scattered by the same scatterer within the IC from the second nuclear test will arrive at a common station with a slight arrival time

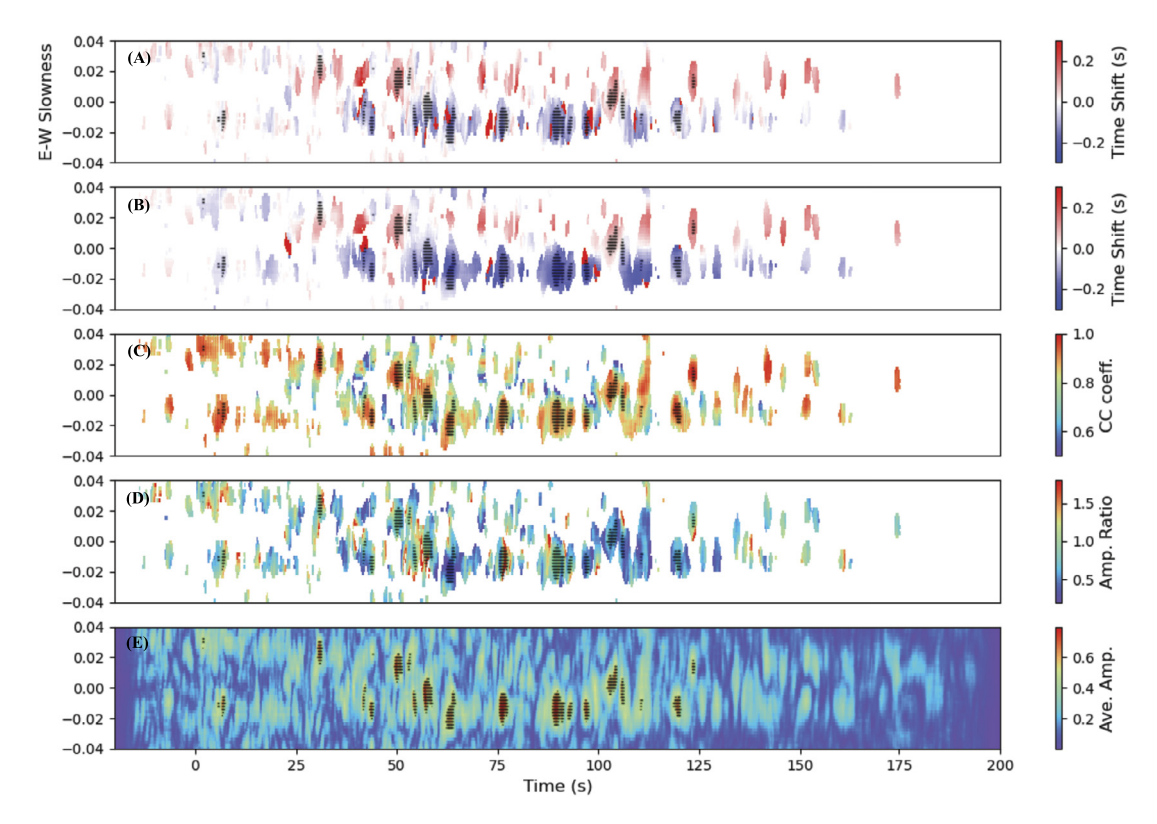


Fig. 2. Energy blips selections shown against roughly transverse slowness and arrival time relative PKiKP. This slice has a fixed N-S slowness of 0.01 s/km. (A) & (B) show the time shifts between the beamformed waveforms from two explosive events computed with the method in Vidale [2019] and our CC approach. (C) is the CC coefficients between the beamformed waveforms. (D) is the amplitude ratios of the beamformed waveforms. (E) is the average amplitude. The black dots mark the points that meet the generous criterion as a blip. We discard the values of the time shifts, CC coefficients and amplitude ratios when their corresponding CC coefficients smaller than 0.5 or amplitude ratio is larger than 1.8 or smaller than 0.2.

shift relative to the first test (see Fig. 4C and 4D, Figure S2). In previous studies, the axis of the IC rotation relative to the mantle is assumed the same as the Earth's rotation axis [e.g., Song and Richards, 1996; Vidale, 2019]. Here, the extensive coverage of the IC scatterers and robust measurements of time shifts provide a unique chance to explore both the rotation axis and the amount of rotation.

## 5. Results

We first identify all the HEHC points. There are a total of 6703 points in slowness-delay-time space with our weak selection criterion and 687 points with the stricter criterion. We note that our study focuses on the beamformed seismic energy from the IC scatterers, therefore we only use the points whose trajectories pass through the IC, although conceivably scattering in the outer core and mantle might contribute.

The slownesses of PKiKP phases from global events measured on LASA indicate that there is a tendency for raypaths close to the edges of the IC to have PKiKP slowness observations up to 0.005 s/km greater than the predicted slowness, likely due to lateral mantle structure under LASA [Vidale and Wang, 2020]. We thus apply a previously derived small empirical correction to those slownesses [Vidale and Wang, 2020]. Next, we back-project the high-energy points in the beam to their associated scatterer locations at the ICB or within the IC (see Fig. 4A & 4B). The scatterers on the western side of LASA correspond to the high-energy points of the negative E-W slowness (Fig. 2). The clear negative time shifts for the PKiKP coda arrivals incident from the west indicate that the PKiKP coda waves of the second explosive event arrived earlier than the corresponding waves from the first one. The time shifts are opposite for the scattered waves incident from the east

of LASA (Fig. 2 & 4A). The east-west pattern indicates, for this geometry, that the western scatterers systematically move closer to LASA and the event location, while the eastern ones move away during the time period between the two explosive events. This spatial pattern of the time shifts is consistent with eastwards differential IC rotation, i.e. super-rotation (see Fig. 4).

For comparison with the observed arrival time shifts, we compute the pattern and amplitude of the time shifts that would arise from a 1° IC super-rotation of the scatterers relative to the mantle, with the rotation pole constrained to coincide with Earth's rotation pole (Fig. 4C and 4D, and Figure S2). We derive the travel time changes by 1D ray-tracing of the iasp91 model [Kennett and Engdahl, 1991].

The comparison of the observed time shifts with the predicted time shifts for the  $1^{\circ}$  super-rotation shows a clear linearity (see Fig. 4E & 4F). We use the L1-norm misfit to search for the best-fitting rotation angle to find the best linear fit. We force the intersect to be 0, as would be the case for a pure rotation. This procedure fixes the origin time difference between the two explosive events and searches for the best rotation angle. We note that Vidale [2019] used only the greater aperture of stations from 1971 explosion to estimate slownesses, which may (or may not) reduce scatter at the expense of less uniform and comprehensive analysis.

Accounting for scatterers at all the depths, the best-fitting rotation rate is 0.100°/year, slightly larger than 0.07°/year in previous study [Vidale, 2019]. The increased estimate arises because we here consider the depths of the scatterers, which were assumed to be shallow in the IC in the previous study. The time shifts measured for the scatterers remain similar, but for deeper scatterers at smaller radii from the center of Earth, larger angular rotation

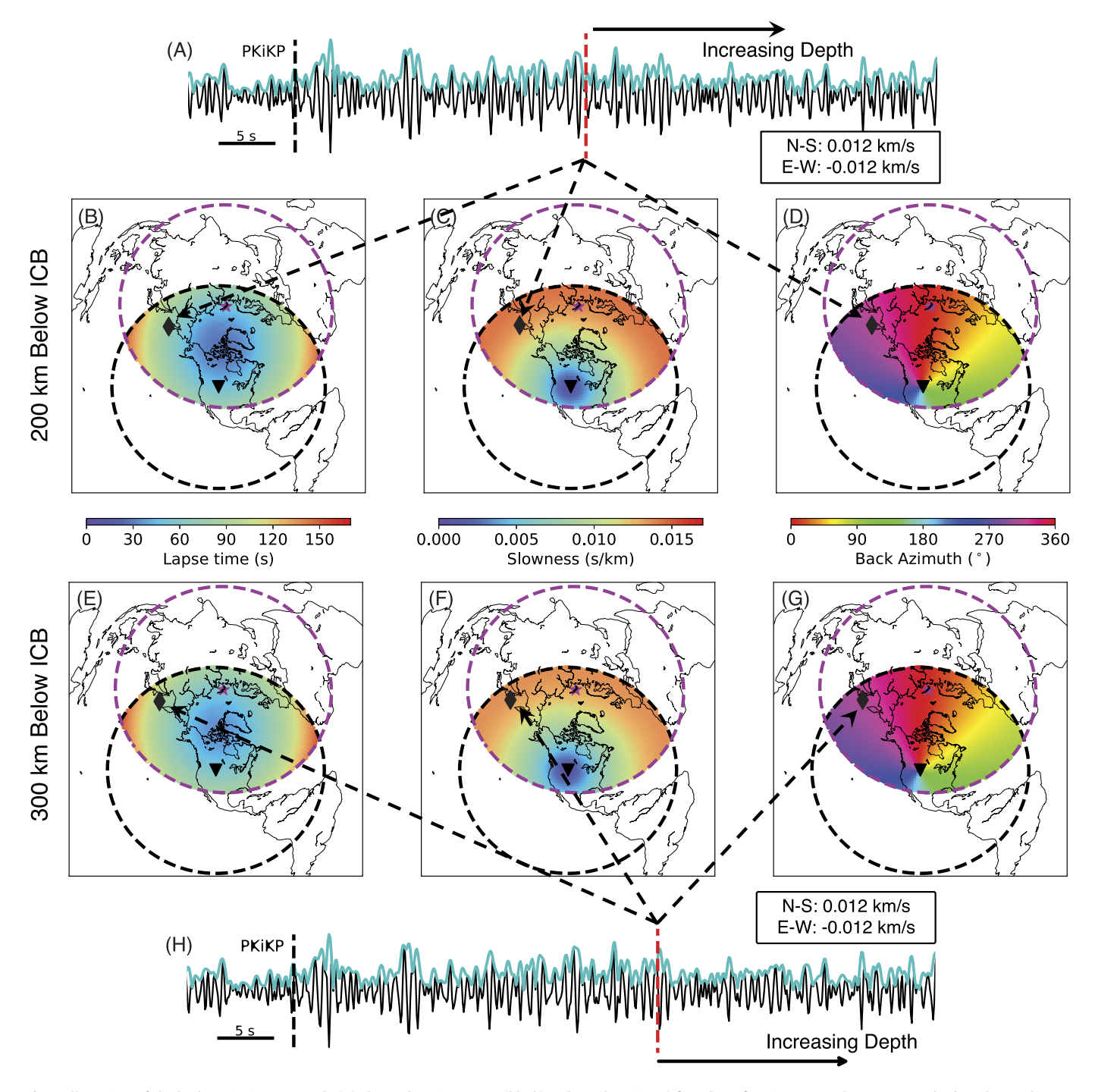


Fig. 3. Illustration of the back-projection approach. (A) shows the seismogram (black) and envelope (cyan) from beamforming at N-S slowness 0.012 km/s and E-W slowness -0.012 km/s. The red dashed line marks energy corresponding to a particular scattering volume in the IC at 200 km below the ICB. (B), (C) and (D) show the lapse time after PKiKP, total slowness, and back-azimuth for scattering at this location 200 km below the ICB. The black diamond indicates the location of such a resolved scatterer. The black triangle shows the location of LASA and black dashed line indicates the outline of IC scatterers that would be visible at LASA from events everywhere. The magenta star indicates the source location, and the magenta dashed line shows the outline of the potential IC scatterers illuminated by this source that would be visible, given arrays everywhere. (E)-(H) show the scattering volume in the IC at 300 km below the ICB similar to (A)-(D). This figure illustrates that the PKiKP coda energy at late lapse time are scattered by the deep scatterers within the IC.

is necessary to match the observed time shifts (Fig. 4C and 4D, and Figure S2). It should be noted that our work mapping the 3D distribution of scatterers [Vidale and Wang, 2020] has provided a firmer basis for placing scatterers deep in the IC.

However, we prefer the slightly different solution obtained ignoring the time shifts for the deepest scatterers. Figs. 4E and 4F reveal that the observed time shifts for the deepest scatterers are systematically smaller than the predicted ones. This may

arise from limitations in slowness resolution due to the finite frequency of scattered waves, velocity structure errors, or multiple scattering, as we note below in the discussion. Thus, we prefer the slightly slower rotation rate of  $0.096\pm0.008^{\circ}$ /year, which incorporates scatterers at only depths shallower than 300 km. To estimate the confidence of the rotation rate, we apply a bootstrapping technique [Efron and Tibshirani, 1991]. We randomly pick 300 out of the total 515 shallow scatterers (<300 km) and estimate the ro-

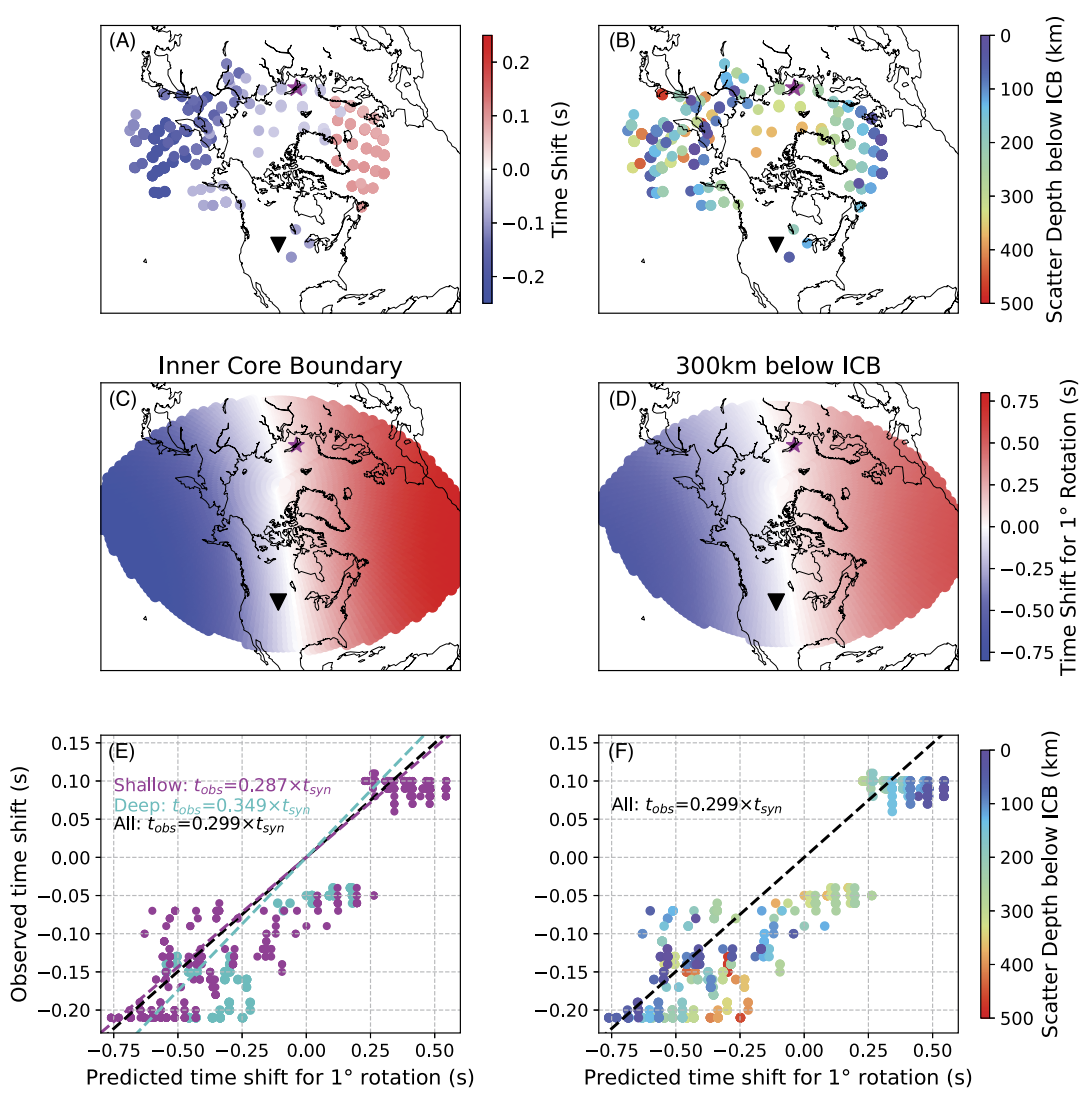


Fig. 4. Distribution of time shifts and depths of the scatterers. (A) and (B) show the time shifts and depths of the single high-energy points. (C) and (D) show the distribution of the predicted time shifts assigned to the scatterers located at different depths assuming the IC rotates eastward  $1^{\circ}$  relative to the mantle. (E) shows the time shifts for the scatterers versus the predicted time shifts for a  $1^{\circ}$  rotation. Magenta points indicate the shallow scatterers (< 300 km) and magenta dashed line shows the linear fitting, and the cyan points show the case for deep scatterers. Black dashed line illustrates the best linear fit for all the scatterers. (F) shows the time shifts of scatterers versus the predicted time shifts for  $1^{\circ}$  IC rotation colored by the depths. Black line is the same as in (E).

tation rate. We repeat this procedure 200 times to estimate the uncertainty of the rotation rate.

## 6. Exploration of remaining misfit

The misfits between the predicted and observed time shifts with the depths and average amplitudes of the scatterers are shown in Fig. 5. The comparison with the depths shows the mean misfits deviate from zero with bias for the scatterers deeper than 300 km. After removal of the arrivals scattered more than 300 km below the ICB, trends of misfit are unbiased (Fig. 5A & 5B). The comparison with the average amplitudes shows the misfits significantly increase below the average amplitude 50%, consistent with our selection criterion, which presumes lower quality for relatively small arrivals. For this reason, in this study, we prefer to omit the time delays of the deepest scatterers (> 300 km) in interpreting the rotation rate and rotation axis.

We offer three possible sources of the misfits. First, we applied a slowness correction to resolve the absolute slowness, motivated by the comparison of the observed and predicted PKiKP slownesses for 73 earthquakes and explosions [Vidale and Wang, 2020]. The

predictions systematically underestimated the observed slowness near the PKiKP slowness rim of the IC. This correction is empirical but well-based on inspecting many PcP and PKiKP arrivals within epicentral distance 100°, but still only an approximation [Vidale and Wang, 2020]. Second, in this study, we assume only single scattering to locate the scatterers in the IC, encouraged by the long mean free paths computed from the scattering estimated by previous studies being much longer than the maximum depths of visible scattering (500 km) [Vidale and Wang, 2020]. Multiple scattering might occur amidst strong heterogeneities, especially for the deeper IC scatterers. The comparison between the depths of the scatterers and the misfits indicates a clear bias for the deep scatterers (>300 km) (see Fig. 5A & 5B). This bias, which appears at 300 km depth and below, might be because the late PKiKP coda energy contains multiple scattering.

So far, we have only interpreted the time shifts of the IC scatterers as differential rotation. However, there are other proposed mechanisms for localized IC temporal changes [Wen, 2006; Cao et al., 2007; Mäkinen and Deuss, 2011; Yao et al., 2015, 2019]. A third potential source of misfit is nonrotational processes, i.e., vertical motion of the ICB [Wen, 2006; Cao et al., 2007; Yao et al., 2015] or

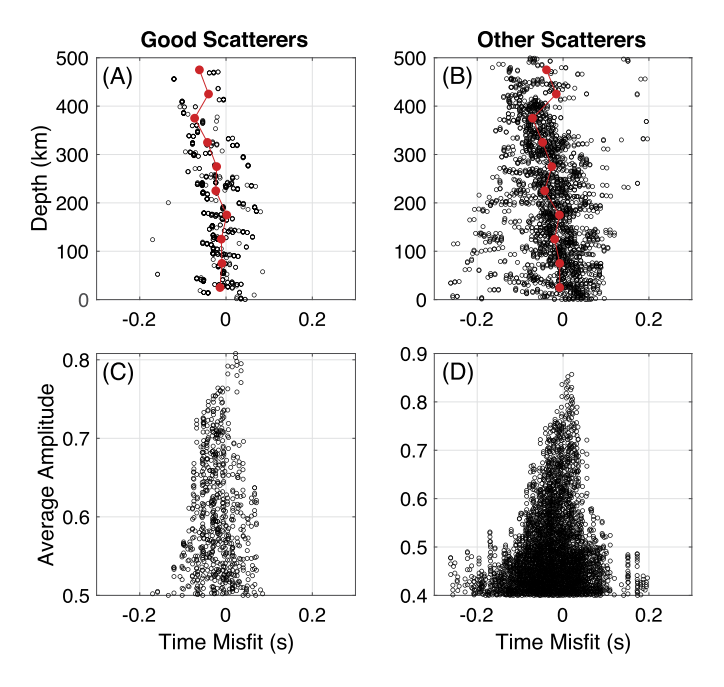


**Fig. 5.** The comparison of the misfits of the observed and predicted time shifts for the inferred rotation axis versus the depths and corresponding average amplitudes of the beamformed seismograms of the scatterers. (A) and (C) show the results for the scatterers that meet the high-level criterion. Red dots show the mean values of the misfits within the 50 km bins in depth. (B) and (D) show the results for the scatterers that meet the low-level criterion but not the high-level one.

structural changes in the IC or OC [Mäkinen and Deuss, 2011; Yang and Song, 2020b]. Time shifts caused by localized media changes could superimpose on the time shifts from IC rotation, generating additional misfit. However, any possible effects of localized temporal changes of IC are not big enough to be identified and separated in this study.

## 7. Rotation axis tilt

In previous studies of IC differential rotation, the axis has been fixed to be the same as the Earth's rotation axis for lack of resolution to test the assumption. However, while this assumption seems likely, it is not dynamically required as far as we know. If the pole of IC differential rotation differs, it is expected to precess in retrograde motion about Earth's rotation pole with an  $\sim$ 15.6-year period, termed IC wobble [Chao, 2017a].

Hence, we grid-search the tilt of the rotation axis, the azimuth of the tilt, and the rotation rate to find the best match to the time shifts of the high-energy points. To accurately estimate the rotation parameters, we first conduct a grid search for the global minimum using large  $2^{\circ} \times 12^{\circ} \times 0.1^{\circ}$  grid elements (latitude  $\times$  longitude  $\times$  rotation angle). Then, we conduct a finer-scale grid search around the coarse-grid global minimum using  $0.5^{\circ} \times 1^{\circ} \times 0.001^{\circ}$  elements. We also apply the same bootstrapping technique to estimate the confidence of the rotation pole and rotation rate. We randomly pick 300 out of the total 515 shallow scatterers (<300 km) and conduct the fine-scale regional grid search to find the best-fitting rotation pole and amount for 200 times to estimate the uncertainties (see Figure S3).

We first examine differential rotation around the Earth's rotation axis. The best-fitting rotation rate is  $0.096\pm0.005^\circ$ /year, which we mentioned above as the estimation from the slope fitting in Fig. 4D. Next, we conduct the global search described in the previous paragraph. Our best-fitting result indicates a rotation axis that is 8° off the geographic north pole, which is located at  $81.7^\circ\pm0.6^\circ$ N and  $36^\circ\pm16.5^\circ$ W with the rotation rate as

 $0.125^{\circ}\pm0.024^{\circ}/\text{year}$  (see Fig. 6). The results of the global grid search and the bootstrapping technique show there are a range of the rotation poles and rotation rates are possible with similar misfit (Fig. 6 and Figure S3). The uncertainty of the longitude ( $\sim$ 250 km) from the bootstrapping test is relatively larger than the uncertainty of the latitude ( $\sim$ 70 km) (see Figure S3). We note that the uncertainties will be underestimates if there are systematic biases such as mentioned below missing in the bootstrap analysis.

Compared to the rotation constrained to be parallel to the Earth's rotation axis, the tilting rotation shows a better fit to the observed time shifts (Fig. 7). For the rotation around the Earth's rotation axis, the distribution of misfits between the observed and predicted time shifts shows a deviation from zero mean. These misfits cannot be explained by the misalignment of the origin times of the two explosions, which has been explored in Vidale [2019] through consideration of alignment of later, less IC sensitive phases.

Tilting of the rotation axis reduces the misfit of the scatterers, especially the ones below northeastern Asia [see Fig. 7D-F, Figure S4]. The scattering strength in this area has been resolved to be strong within 300 km below ICB [Vidale and Wang, 2020]. Therefore, our modeling of the IC scatterer temporal changes may be biased by the multiple scattering. In parallel, there is also a report of large temporal changes in the PKPbc (or PKPab) - PKIKP differential time, which may also indicate localized small-scale lateral variations in the shallow part of the IC (< 300 km) [Yang and Song, 2020b]. However, dynamically, IC differential rotation so far from co-linearity with Earth's rotation is unlikely [Dumberry, 2008]. To better constrain any tilt of the IC rotation axis, more repeating earthquake sequences and large-aperture dense arrays would help by improving the coverage for mapping the IC and reduce artifacts potentially caused by multiple scattering from strong scattering regions, and perhaps localized temporal changes at the ICB and/or within the IC.

## 8. Geodynamical interpretations

IC super-rotation was first predicted in geodynamic simulations driven by the electromagnetic coupling between the IC and convective OC [Gubbins, 1981; Glatzmaier and Roberts, 1996]. However, it is difficult to confidently predict the expected rotation pattern driven by coupling with the gravitational, viscous, and magnetic forces [Aurnou and Olson, 2000]. After initial seismological estimations of the rotation rate of 1-3°/year [Song and Richards, 1996; Su et al., 1996], the rotation rates have decreased to below 0.2°/year [Yang and Song, 2020a], using similar timing changes in PKPbc-PKIKP differential travel times over decades. A decadescale survey of the normal modes infers a rotation rate of 0.13°  $\pm$  0.11°/year [Laske and Masters, 2003].

The hemispheric structural dichotomy of the IC and the inclination of boundaries of the east-west hemispheric boundary may indicate at most weak rotation on the timescale of seismic observations [Waszek et al., 2011]. The geodynamic simulations also suggest that the current seismic observations of faster rotation may come from the small-time-scale IC oscillation superimposed on a large-time-scale steady rotation, depending on the relative influence of viscous, gravitational and magnetic torques [Aubert et al., 2008; Dumberry and Mound, 2010; Waszek et al., 2011]. For example, on a decadal time scale, it is possible that the IC can oscillate at the maximum rate of about 0.1°/year with a 60-year period from a much larger magnetic torque fluctuations [Aubert et al., 2008], consistent with our observation and some previous studies [Laske and Masters, 2003; Vidale, 2019; Yang and Song, 2020a].

A steady six-year oscillation has been resolved in the length of day and geomagnetic field variations [Mound and Buffett, 2006; Holme and De Viron, 2013; Ding and Chao, 2018]. Mantle-inner-

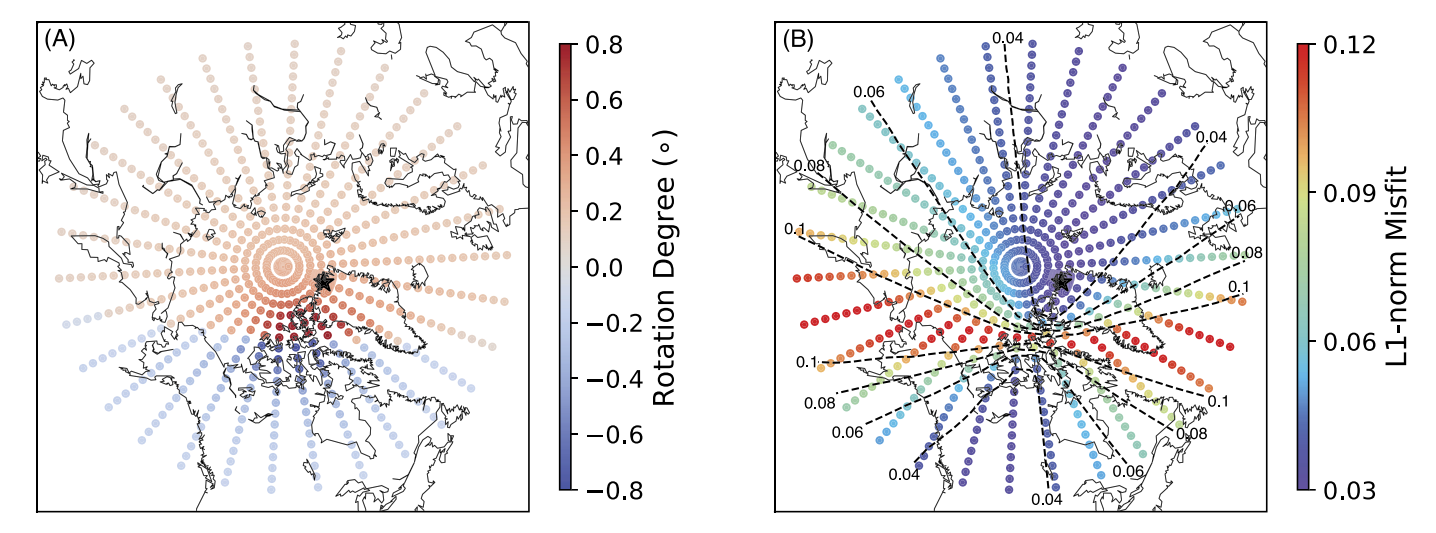


Fig. 6. Grid Search for inferred rotation rates and misfit across possible locations for rotation poles using the shallow scatterers (< 300 km). (A) & (B) are the grid search results for the best-fitting rotation rates and L1-norm misfit for their associated rotation poles, respectively.

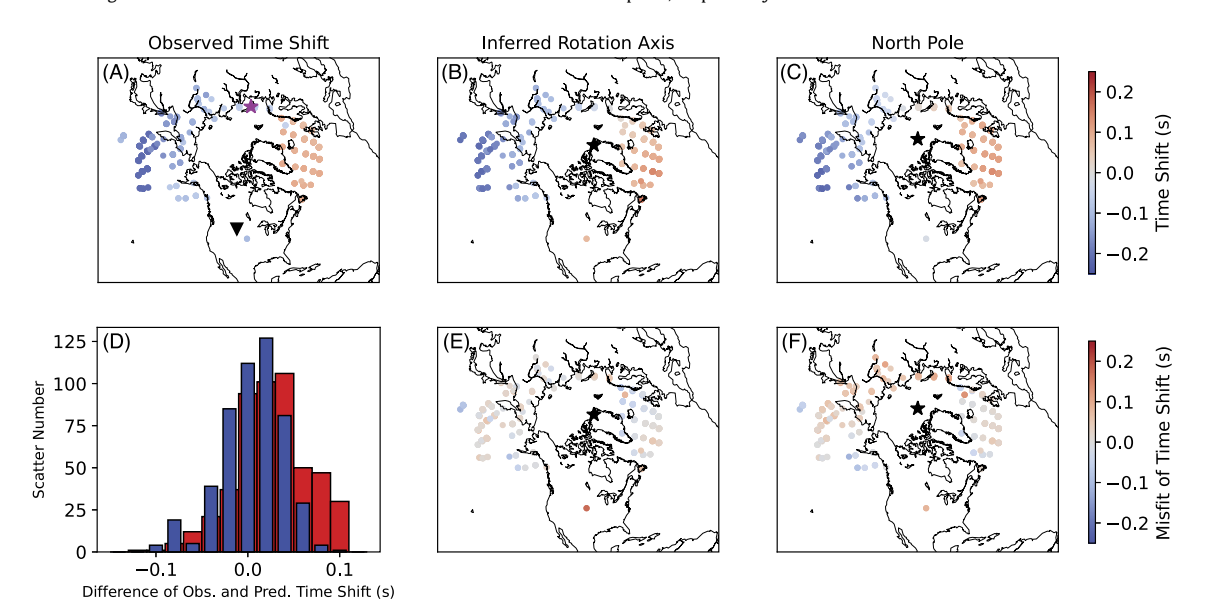


Fig. 7. Comparison of the observed and predicted time shifts for the north pole and inferred rotation axis using the shallow scatterers (< 300 km). (A) shows the distribution of measured time shifts. (B) and (C) show the predicted time shifts assigned to their scatterers' locations for the rotation axis as the inferred rotation axis and the north pole, respectively. (D) illustrates the histograms of the misfit between the observed and predicted time shifts. The blue and red histograms show the misfits for the rotation axis as the inferred rotation axis (B) and north pole (C), respectively. (E) and (F) show the misfit between the observed and predicted time shifts for those two rotation axes, respectively. The black star in each subplot illustrates the location of rotation axis.

core gravitational (MICG) coupling has been proposed to explain the 6-year axial libration, which is driven by degree-two density structure of the mantle and IC and the equatorial ellipticities of the CMB and ICB [Ding and Chao, 2018]. The predicted IC axial rotation and our rotation are both super-rotation from 1971 to 1974 (see Figure S5), and our estimated rotation angle is roughly consistent with the predicted value [Chao, 2017b]. The MICG coupling only considers the gravitational coupling, therefore the rate discrepancy might easily arise from an over-simplified coupling model. This idea of MICG coupling does not require fixing the rotation axis to match Earth's rotation axis, given the asymmetric structure of the lower mantle [Garnero et al., 2016] and also asymmetry in the IC, so the IC differential rotation axis may deviate from the Earth's rotation axis, as we considered above, but further studies would be needed for definitive models and observations.

In summary, based on the refined beamforming, objective thresholding, and improved correlation, we measure the time shifts of the high-energy and highly-coherent scattered energy within the IC scattered waves, radiated by twin nuclear explosions. We applied the back-projection technique to locate the corresponding scatterers. Aided by the locations, including depths, of the IC scatterers, we explore the IC rotation considering both a fixed and free rotation axis. Our results show a tightly constrained rotation of 0.29° from 1971 to 1974 if differential rotation aligns with Earth's rotation axis, or if not, a more uncertain rotation of 0.37° around an axis that is tilted about 8° from Earth's rotation axis.

## **CRediT authorship contribution statement**

Conception and design of study: Wei Wang, John E. Vidale; Analysis of data: Wei Wang, John E. Vidale;

Drafting the manuscript: Wei Wang, John E. Vidale;

WW and JV each equally contributed to project design, methodology, data processing and manuscript preparation. Both persons who meet authorship criteria are listed as authors, and both authors certify that they have participated sufficiently in the work to

take public responsibility for the content, including participation in the concept, design, analysis, writing, or revision of the manuscript. Furthermore, each author certifies that this material or similar material has not been and will not be submitted to or published in any other publication before its appearance in the Earth and Planetary Science Letter.

### **Declaration of competing interest**

The authors declare that they have no known competing financial interests or personal relationships that could have appeared to influence the work reported in this paper.

## Data availability

The LASA data are available online (https://github.com/JohnVidale/LASA\_data), and we anticipate that it will soon be available through IRIS.

#### Acknowledgements

We thank the editor Hans Thybo, Xiaodong Song, and another an anonymous reviewer for insightful and fruitful comments, which help greatly improve the manuscript. Paul Earle recovered the LASA data from deteriorating nine-track tapes in the 1990s, and Steven Gibbons provided the LASA data from his archives. The authors want to thank Ben Chao and Jiayuan Yao for the fruitful discussions. This study is supported by NSF grant EAR-2041892.

#### Appendix A. Supplementary material

Supplementary material related to this article can be found online at https://doi.org/10.1016/j.epsl.2021.117214.

#### References

- Aubert, J., Amit, H., Hulot, G., Olson, P., 2008. Thermochemical flows couple the Earth's inner core growth to mantle heterogeneity. Nature 454 (7205), 758–761.
   Aurnou, J., Olson, P., 2000. Control of inner core rotation by electromagnetic, gravi-
- tational and mechanical torques. Phys. Earth Planet. Inter. 117 (1-4), 111–121. Cao, A., Masson, Y., Romanowicz, B., 2007. Short wavelength topography on the
- inner-core boundary. Proc. Natl. Acad. Sci. USA 104, 31–35.
  Cao, A., Romanowicz, B., 2007. Locating scatterers in the mantle using array analysis
- Cao, A., Romanowicz, B., 2007. Locating scatterers in the mantle using array analysis of PKP precursors from an earthquake doublet. Earth Planet. Sci. Lett. 255 (1–2), 22–31.
- Chao, B.F., 2017a. Dynamics of the inner core wobble under mantle inner core gravitational interactions. J. Geophys. Res., Solid Earth 122, 7437–7448.
- Chao, B.F., 2017b. Dynamics of axial torsional liberation under the mantle-inner core gravitational interaction. J. Geophys. Res., Solid Earth 122, 560–571.
- Creager, K.C., 1997. Inner core rotation rate from small-scale heterogeneity and timevarying travel times. Science 278 (5341), 1284–1288.
- Deuss, A., 2014. Heterogeneity and anisotropy of Earth's inner core. Annu. Rev. Earth Planet. Sci. 42 (1), 103–126.
- Ding, H., Chao, B.F., 2018. A 6-year westward rotary motion in the Earth: detection and possible MICG coupling mechanism. Earth Planet. Sci. Lett. 495, 50–55.
- Dumberry, M., 2008. Gravitational torque on the inner core and decadal polar motion. Geophys. J. Int. 172, 903–920.
- Dumberry, M., Mound, J., 2010. Inner core-mantle gravitational locking and the super-rotation of the inner core. Geophys. J. Int. 181 (2), 806–817.
- Efron, B., Tibshirani, R., 1991. Statistical data analysis in the computer age. Science 253, 390–395.
- Frosch, R.A., Green, P.E., 1966. The concept of the large aperture seismic array. Proc. R. Soc. Lond. 290, 368–384.

- Frost, D.A., Rost, S., Selby, N.D., Stuart, G.W., 2013. Detection of a tall ridge at the core-mantle boundary from scattered PKP energy. Geophys. J. Int. 195 (1), 558–574.
- Garnero, E., McNamara, A., Shim, S.H., 2016. Continent-sized anomalous zones with low seismic velocity at the base of Earth's mantle. Nat. Geosci. 9, 481–489.
- Glatzmaier, G.A., Roberts, P.H., 1995. A three-dimensional convective dynamo solution with rotating and finitely conducting inner core and mantle. Phys. Earth Planet. Inter. 91 (1–3), 63–75.
- Glatzmaier, G.A., Roberts, P.H., 1996. Rotation and magnetism of Earth's inner core. Science 274 (5294), 1887–1891.
- Gubbins, D., 1981. Rotation of the inner core. J. Geophys. Res. 86 (B12), 11695–11699.
- Holme, R., De Viron, O., 2013. Characterization and implications of intradecadal variations in length of day. Nature 499 (7457), 202–204.
- Kennett, B.L.N., Engdahl, E.R., 1991. Travel times for global earthquake location and phase association. Geophys. J. Int. 105, 429–465.
- Laske, G., Masters, T.G., 2003. The Earth's free oscillations and the differential rotation of the inner core. In: Veronique Dehant, K.C.C., Karato, S.-I., Zatman, S. (Eds.), Earth's Core: Dynamics, Structure, Rotation. In: AGU Dynamics Series, vol. 31. American Geophysical Union, Washington, DC, pp. 5–21 (Chap. 1).
- Lindner, D., Song, X., Ma, P., Christensen, D.H., 2010. Inner core rotation and its variability from nonparametric modeling. J. Geophys. Res. 115, B04307.
- Mäkinen, A.M., Deuss, A., 2011. Global seismic body-wave observations of temporal variations in the Earth's inner core, and implications for its differential rotation. Geophys. J. Int.
- McFadden, P.L., Merrill, R.T., 1984. Geodynamo energy source constraints from palaeomagnetic data. Phys. Earth Planet, Inter. 43, 22–23.
- Mound, J., Buffett, B., 2006. Detection of a gravitational oscillation in length-of-day. Earth Planet. Sci. Lett. 243, 383–389.
- Poupinet, G., Souriau, A., Coutant, O., 2000. The existence of an inner core superrotation questioned by teleseismic doublets. Phys. Earth Planet. Inter. 118 (1–2), 77–88.
- Song, X., Richards, P.G., 1996. Seismological evidence for differential rotation of the Earth's inner core. Nature 382 (6588), 221–224.
- Souriau, A., 1998a. Detecting possible rotation of Earth's inner core, response to comments by P.G. Richards, X.D. Song, and A. Li. Science 282, 1227a.
- Souriau, A., 1998b. Is the rotation real? Science 281 (5373), 55-56.
- Souriau, A., Poupinet, G., 2000. Inner core rotation: a test at the worldwide scale. Phys. Earth Planet. Inter. 118 (1–2), 13–27.
- Su, W.-J., Dziewonski, A.M., Jeanloz, R., 1996. Planet within a planet: rotation of the inner core of Earth. Science 274 (5294), 1883–1887.
- Tkalčić, H., Young, M., Bodin, T., Ngo, S., Sambridge, M., 2013. The shuffling rotation of the Earth's inner core revealed by earthquake doublets. Nat. Geosci. 6 (6), 497–502
- Vidale, J.E., 2019. Very slow rotation of Earth's inner core from 1971 to 1974. Geophys. Res. Lett. 46 (16), 9483–9488.
- Vidale, J.E., Dodge, D., Earle, P.S., 2000. Slow differential rotation of the Earth's inner core indicated by temporal changes in scattering. Nature 405, 445–448.
- Vidale, J.E., Wang, W., 2020. An map of inner core scatterers from beamforming the LASA array. In: AGU Fall Meeting 2020. AGU.
- Waszek, L., Irving, J., Deuss, A., 2011. Reconciling the hemispherical structure of Earth's inner core with its super-rotation. Nat. Geosci. 4 (4), 264–267.
- Wen, L., 2000. Intense seismic scattering near the Earth's core mantle boundary beneath the Comoros hotspot. Geophys. Res. Lett. 27 (22), 3627–3630.
- Wen, L., 2006. Localized temporal change of the Earth's inner core boundary. Science 314, 967–971.
- Xin, D., Song, X., Wang, T., 2015. Localized temporal variation of Earth's inner-core boundary from high-quality waveform doublets. Earthq. Sci. 28 (3), 175–185.
- Yang, Y., Song, X., 2020a. Origin of temporal changes of inner-core seismic waves. Earth Planet. Sci. Lett. 541, 116267.
- Yang, Y., Song, X., 2020b. Temporal changes of the inner core from globally distributed repeating earthquakes. J. Geophys. Res., Solid Earth, e2019JB018652.
- Yao, J., Sun, L., Wen, L., 2015. Two decades of temporal change of Earth's inner core boundary. J. Geophys. Res., Solid Earth 120, 6263–6283.
- Yao, J., Tian, D., Sun, L., Wen, L., 2019. Temporal change of seismic Earth's inner core phases: inner core differential rotation or temporal change of inner core surface? J. Geophys. Res., Solid Earth 124 (7), 6720–6736.
- Zhang, J., Song, X., Li, Y., Richards, P.G., Sun, X., Waldhauser, F., 2005. Geophysics: inner core differential motion confirmed by earthquake waveform doublets. Science 309 (5739), 1357–1360.